Bioactive photocrosslinkable resin solely based on refined decellularized small intestinal submucosa for digital light processing 3D printing of *in vitro* tissue mimics

Laura Elomaa,[1,*] Lorenz Gerbeth,[2,3] Ahed Almalla,[1] Nora Fribiczer,[4] Peter Tang,[5] Karl Hillebrandt,[5,6] Igor M. Sauer,[5,7] Sebastian Seiffert,[4] Britta Siegmund,[2] Marie Weinhart[1,7,8,*]

[1]*Institute of Chemistry and Biochemistry, Freie Universität Berlin, Takustr. 3, 14195 Berlin, Germany*

[2]*Department of Gastroenterology, Infectious Diseases and Rheumatology (including Nutrition Medicine), Charité – Universitätsmedizin Berlin, corporate member of Freie Universität Berlin and Humboldt-Universität zu Berlin, Hindenburgdamm 30, 12203 Berlin, Germany*

[3]*Institute of Biotechnology, Technische Universität Berlin, Gustav-Meyer-Allee 25, 13355 Berlin, Germany*

[4]*Department of Chemistry, Johannes Gutenberg University Mainz, Duesbergweg 10-14, 55128 Mainz, Germany*

[5]*Experimental Surgery, Department of Surgery, CCM|CVK, Charité – Universitätsmedizin Berlin, Augustenburger Platz 1, 13353 Berlin, Germany*

[6]*Berlin Institute of Health at Charité – Universitätsmedizin Berlin, BIH Biomedical Innovation Academy, BIH Charité Clinician Scientist Program, Charitéplatz 1, 10117 Berlin, Germany*

[7]*Cluster of Excellence Matters of Activity. Image Space Material funded by the Deutsche Forschungsgemeinschaft (DFG, German Research Foundation) under Germany´s Excellence Strategy – EXC 2025*

[8]*Institute of Physical Chemistry and Electrochemistry, Leibniz Universität Hannover, 30167 Hannover, Germany*

* Corresponsing authors: laura.elomaa@fu-berlin.de and marie.weinhart@fu-berlin.de

Abstract

Three-dimensionally (3D) printed tissue mimics are a unique *in vitro* platform for studying human pathophysiology in a more physiologically relevant manner compared to oversimplified 2D cell cultures and complex animal models. Furthermore, they can be used for replacing parts of damaged tissue or organs. However, their 3D printing requires an availability of materials that at the same time show a high level of biomimicry and also have a suitable viscosity profile and crosslinking kinetics for the desired printing technique. We developed a new biomimetic material for the digital light processing stereolithography (DLP SLA) 3D printing by solubilizing and functionalizing porcine small intestine submucosa (dSIS) into photocrosslinkable dSIS methacrylamide (dSIS-MA) and by subsequently formulating it into a bioactive 3D printing resin. The concentration of 1.5 weight-% of dSIS-MA yielded desired viscosity and photocrosslinking kinetics, and the 3D printing of the resin resulted in fully transparent and highly swelling dSIS-MA hydrogels with a stiffness resembling native intestinal tissue. Both human small intestine organoid-derived undifferentiated primary cells and immortalized human Caco-2 cells grew to confluency on the 3D printed hydrogels without additional cell-adhesive precoating and formed continuous tight junctions, thereby demonstrating the suitability of the material for growing a (personalized) intestinal epithelium. Furthermore, both immortalized human HT29-mtx cells and a part of the human primary intestinal cells produced mucin 5AC, demonstrating bioactivity by early differentiation of these cells on the photocrosslinked dSIS-MA hydrogels. The new dSIS-MA resin was 3D printed into intestine-mimicking scaffolds that desirably guided the seeded human intestinal cells to grow along the 3D villi architectures. The detected cell compatibility of the new dSIS-MA material combined with its high printability and biomimicry indicated that this new material can be an excellent tool for modelling and reproducing native tissue architectures where enhanced physiological relevancy is desired.

1. Introduction

A digital light processing stereolithography (DLP SLA) is a powerful but still often underrated three-dimensional (3D) printing process in biofabrication. It allows scalable and reproducible generation of physiologically relevant *in vitro* tissue mimics with a higher resolution compared to commonly used extrusion-based 3D printing.[1] These tissue mimics can further be personalized by applying the respective computer-aided design and patient-derived cells to allow studies of patient-specific tissue development and homeostasis as well as *in vitro* disease modelling. With a suitable resin but without a big investment in expensive bioprinters, complex tissue-like architectures can be fabricated with a reasonable resolution in any lab or medical facility using the commercially available, low-cost DLP SLA printers. In biomedical 3D printing, the photocrosslinkable resin for the DLP SLA printing would ideally replicate the properties of native extracellular matrix (ECM) to provide cells with a desirable macroenvironment. The native ECM is composed of a complex mixture of macromolecules, especially proteins and proteoglycans, that are important for its structural and mechanical properties as well as for cell attachment and signaling.[2] Furthermore, the cell signaling molecules, especially growth factors, and the physical properties of the ECM guide the migration and differentiation of cells in their matrix.[3] However, the high complexity and tissue specificity of native ECM are not closely resembled by current ECM-mimicking 3D printing resins based on polymers such as methacrylated polyethylene glycol of gelatin methacryloyl (GelMA) that are still fairly simple compared to their native counterpart. An attractive approach to tackle this challenge is to base the 3D printing resin on native decellularized ECM (dECM) instead of using simplified synthetic ECM mimics. As the dECM recapitulates the native tissue-specific environment even after the decellularization,[4] it is an ideal candidate for use as bioactive material in biomedical DLP SLA printing.

Decellularized small intestinal submucosa (dSIS) is an excellent dECM material for biofabrication of cell culture substrates due to its high biological activity and fibrous 3D microenvironment.[5] Previously, dSIS patches have been successfully used for various surgical procedures, such as tendon and corneal repair, [6,7] and they have been studied as *in vitro* intestinal models when seeded with Caco-2 cells or human primary intestinal epithelial cells.[8–10] However, the flat dSIS sheets neither allow their extrusion-based nor SLA-based 3D printing into self-standing tissue mimics with fine-resolved 3D features. For this purpose, the dSIS sheet must first be ground into small particles or fully solubilized. To enable their extrusion printing, Kim *et al*.[11] ground the dSIS sheets into a fine powder and mixed it with collagen solution, which they then printed into 3D hydrogel constructs. Elsewhere, Shia *et al*.[12] obtained extrudable dSIS-based ink by solubilizing a decellularized porcine small intestine via enzymatic digestion in acidic pepsin solution. The 3D printing of these extrudable dSIS inks, as well as other dECM-based inks, relies on their physical gelation when the material is deposited into physiological temperature and pH conditions, which often requires assistance from blended polymer additives also capable of gelation.[13] While the physical dSIS hydrogels are cell adhesive materials, the traction forces and protease production from seeded or embedded cells can rapidly deform the unsupported dSIS hydrogels, resulting in the lack of mechanical strength.[14]

In contrast to the extrusion bioprinting, in SLA 3D printing the solubilized dSIS is first functionalized to yield a photocrosslinkable polymer, and because of the strengthening effect of the photocrosslinking, the 3D printing resin can be formulated without further supportive materials. Previously, the photocrosslinking of dSIS hydrogels was attempted by mixing the solubilized dSIS with riboflavin.[15] However, the photocrosslinking failed to enhance the gelation and increase the material stiffness, which was explained by the inaccessible pendant amine groups in the entangled, partly undigested dSIS. More successfully, the photocrosslinking of other dECM types has been enabled by functionalizing them with double bond-containing methacryl groups. Visser *et al*.[16] and Rothrauff *et al*.[17] functionalized tendon-, cartilage-, and meniscus-derived dECM with methacrylic anhydride and photocrosslinked them into hydrogels mixed with gelatin methacryloyl (GelMA), albeit without applying the material in 3D printing. Furthermore, Ali *et al*.[18] and Kim *et al.*[19] methacrylated kidney-derived dECM porcine and skeletal muscle tissue-derived dECM, respectively, and formulated extrudable inks by mixing them with gelatin, hyaluronic acid, and glycerol or with poly(vinyl alcohol). However, the use of dECM-based resins in the SLA printing has been very limited. Among the very few reports, solubilized but unmodified dECM blended with photocrosslinkable GelMA has been used in SLA printing to form one-layer cellular structures[20] and we have used methacryl-functionalized liver dECM blended with methacrylated poly(ε-caprolactone) for the multi-layer SLA printing.[21] Interestingly, there are no earlier reports of SLA-based 3D printing of any type of photocrosslinkable dECM as a sole material. In our current work, we solubilized porcine dSIS via pepsin digestion and synthesized photocrosslinkable dSIS methacryloyl (dSIS-MA) that we further formulated into an aqueous bioactive 3D printing resin. We demonstrated the 3D printing capacity of this new dSIS-MA resin by printing intestine-mimicking scaffolds with a visible light DLP SLA printer. In our study, the resulting hydrogel scaffolds supported the biofabrication of preliminary small intestinal tissue-mimics after their population with human organoid-derived undifferentiated intestinal epithelial cells.

2. Material and Methods

2.1 Materials

Sodium dodecyl sulfate, Triton™ X-100, pepsin from porcine gastric mucosa (>2.5 kU/mg), proteinase K from Tritirachium album (>30 U/mg), papain, 1,9-dimethyl-methylene blue dye, glycine, chondroitin sulfate, methacrylic anhydride, 2,4,6- trinitrobenzene sulfonic acid (TNBS), and chloramine-T were purchased from Sigma and used as received. Ehrlich's reagent was prepared from *p*-dimethylaminobenzaldehyde (Sigma) freshly before use. PBS was prepared by dissolving tablets (Sigma Aldrich, 0.01 M phosphate buffer without Ca/Mg) in milli-Q water to yield pH 7.4. SpectraPor® dialysis tubing made from regenerated cellulose with a molecular weight cut-off (MWCO) of 3.5 kDa were purchased from Carl Roth GmbH + Co. KG (Karlsruhe). Lithium phenyl-2,4,6-trimethylbenzoylphosphinate (LAP) photoinitiator was synthesized as described before.[16]. Pierce® RIPA buffer and a protease/phosphatase inhibitor cocktail was purchased from Thermo Fisher. Human colorectal adenocarcinoma Caco-2 cells were purchased from ATCC (HTB-37TM) and human colon-derived, mucus

secreting HT29-mtx-E12 cells from European Collection of Authenticated Cell Cultures via Sigma Aldrich (ECACC 12040401). High glucose basal medium (DMEM, Gibco), fetal bovine serum (FBS, Biochrom), bovine serum albumin (Serva), penicillin-streptomycin (Life Technologies), non-essential amino acid solution (100X, Sigma), PrestoBlue™ assay (Thermo Fisher), rabbit anti-human ZO-1 primary antibody (Abcam), goat anti-rabbit IgG Alexa Fluor 647® secondary antibody (Abcam), mouse anti-human MUC5AC primary antibody (LifeTech), goat anti-mouse IgG Alexa Fluor 488® secondary antibody (LifeTech), Hoechst 33342 DNA-intercalating dye (Thermo Fisher), and Phalloidin-Atto 647® (Sigma Aldrich) were used in cell culture as diluted according to the provided protocols.

Human primary epithelial cells were obtained from ileal biopsy specimen of Crohn's disease patients (approved by the ethical committee of the Charité – Universitätsmedizin Berlin). Chelating buffer for isolation of human ileal crypts was made by dissolving D-sorbitol (Carl Roth), sucrose (Thermo Fisher Scientific), ethylenediaminetetraacetic acid (EDTA, Merck), and 1,4-dithiothreitol (DTT, Carl Roth) in PBS (Gibco). Antibiotic stock solutions of ciprofloxacin (Fresenius), fluconazol (B. Braun), gentamycin (Ratiopharm), and primocin (Invivogen) were diluted directly in buffer or medium to obtain desired working concentrations. Advanced DMEM/F-12 with GlutaMAX supplement (Gibco), HEPES buffer (Gibco), and TrypLE solution (Gibco) for culture and passaging of human organoids were used as received. Growth factor stock solutions were obtained by dissolving lyophilized recombinant human epidermal growth factor (Peprotech) and recombinant human R-Spondin 1 (R&D Systems) in 0.1% BSA/PBS solution. Nicotinamide (Merck) and Y-27632 (Abmole) were dissolved in PBS, A83-01 (Merck) and SB 202190 (Merck) were dissolved in DMSO, and human gastrin I (Merck) was dissolved in 0.1% NaOH prior to use. WRN-conditioned medium was produced with L-WRN cells (ATCC CRL-3276) as described previously.[22] Matrigel (Corning) for organoid culture or material coating was used as received. For the standard insert system, Millicell® cell culture inserts (12 mm diameter), polycarbonate membranes with 0.4 µm pore size from Merck Millipore were used.

2.2 Decellularization and enzymatic digestion of small intestinal submucosa (SIS) and synthesis of photocrosslinkable dSIS methacrylamide (dSIS-MA)

A porcine small intestine was explanted after an experiment approved by the State Office of Health and Local Affairs (LAGeSo, Berlin, Germany) and decellularized with a chemical treatment. Briefly, the explanted small intestine was preserved in 1% gentamycin/PBS solution overnight at 4°C after its thorough rinsing. Next day, the mucosa and serosa were mechanically removed, after which the intestine segments were turned upside down and filled first with 1% SDS for 2 h and then with 1% Triton-X for 24 h. After the two-step chemical decellularization at RT, the segments were rinsed and incubated with PBS for another 1 h. Finally, the segments were immersed in fresh 1% gentamycin/PBS solution for 5 times and in the end in PBS. The resulting colorless dECM was further solubilized following a protocol from Rothrauff *et al.* [17] First, the cryo-frozen dSIS was ground with a mortar and a pestle, after which the resulting material was digested in acidic pepsin solution (1 mg of pepsin and 10 mg of dry dSIS in 1 mL of 0.01 N HCl, pH 2) at RT for two days. The pepsin digestion was then

stopped by adjusting the pH to 9 with 1 N NaOH solution. Afterwards, the digested polymer was methacryl-functionalized by sequential (6 times) addition of methacrylic anhydride (MAAh) into the solution during 3 h (in total 1 mL of MAAH per 1 g of dSIS), while the pH was maintained at pH 9 with addition of 1 N NaOH. Afterwards, the pH was adjusted to 7.4 and the resulting dSIS-MA polymer was dialyzed against PBS for one day and then distilled water for six days, after which it was lyophilized.

2.3 Biochemical characterization of SIS, dSIS, and dSIS-MA

The DNA content in SIS and digested dSIS was detected with an AccuBlue® dsDNA detection kit (Biotium, USA). Before the DNA detection, the tissue was lyophilized until full dryness, after which 50 mg of dry tissue was transferred to 800 µL of extraction buffer (50 mM Tris-HCl, pH 8; 25 mM EDTA, and 400 mM NaCl). Furthermore, 20 µL proteinase K (10 µg/µL, ≥30 units/mg) was added. The tissue extract was incubated overnight at 60 °C under strong shaking, and after centrifugation at 10,000 x g for 10 min, the supernatant was used without further purification for the dsDNA analysis. The fluorescent AccuBlue® reagent was diluted to 1:100 in Tris-EDTA buffer (10 mM Tris-HCl, pH 8; and 1 mM EDTA) and then mixed with the sample at a ratio of 20:1 and further incubated for 15 min in the dark at RT. Supernatants incubated without the presence of fluorescence dye were used as blanks. The fluorescence of triplicate samples was measured using a microplate reader (Infinite® M200 Pro, Tecan) with an excitation of 350 nm and emission of 460 nm in a 96-well plate and the readings were further translated to the weight using a calibration curve. For the quantification of a sulphated glycosaminoglycans (sGAG) content, 10 mg of lyophilized tissue samples was extracted with 0.025 w/v % papain (30000 units/mg) in buffer (20 mM EDTA, 5mM L-cysteine, pH 5.6) overnight at 65°C with vigorous shaking, after which the samples were centrifuged at 1000 x g for 10 minutes. The sGAG content of the supernatant was quantified using the 1,9-dimethyl-methylene blue (DMMB) dye assay according to a previously published protocol.[23] Briefly, DMMB dye solution was first prepared by dissolving 16 mg of DMMB dye, 3.04 g of glycine, 1.6 g of NaCl, and 95 ml of 0.1 M acetic acid and the volume was adjusted with milli-Q water to 1 L (the final pH was 3). Freshly prepared DMMB solution was mixed with the samples at a ratio of 20:2 in 96-well plates, and the absorbance at 525 nm was measured using the microplate reader. The readings were then compared to a standard curve of chondroitin sulfate. For the quantification of hydroxyproline content of SIS and dSIS, 10 mg of lyophilized samples were hydrolyzed overnight at 115°C in 6M HCl. The samples were oxidized with chloramine-T and mixed with Ehrlich's reagent, and their absorbance was measured at a wavelength of 550 nm in a 96 well plate using the plate reader. The total hydroxyproline content was obtained using a hydroxyproline standard curve and was normalized to the dry tissue weight. The growth factors in the SIS ans dSIS tissue was quantified with a Quantibody® human growth factor multiplex ELISA array Q1 (RayBiotech) following the protocol provided by the company. For the assay, 20 mg of lyophilized tissue was shaken overnight in 1 mL RIPA lysis buffer containing protease/phosphatase inhibitor cocktail at 4 °C, and after centrifugation at 60,000 x g for 5 min, the supernatant was used as a sample in the Quantibody® assay. The fluorescence reading of the array was read at 532 nm using GenePix®

4300A Microarray scanner (Molecular Devices, USA), and the concentration of the growth factors was quantified against linear calibration curves of the respective growth factors.

2.4 Formulation of a dSIS-MA resin and 3D printing of hydrogels by DLP SLA

To formulate the dSIS-MA into a bioactive 3D printing resin, it was dissolved in 0.01N NaOH with concentrations of 1.5, 2, 2.5, and 3 weight-% (wt-%) with 1 wt-% of LAP photoinitiator and 0.05 wt-% of orange food color (Wesentlich, Germany). The formulated resin was then homogenized with an electronic dispenser (IKA ULTRA-TURRAX® T10). Disc-shaped samples (diameter of 8 mm and thickness of 2 mm, unless otherwise stated) for characterization of the physicochemical and biological properties of the crosslinked dSIS-MA hydrogels as well as intestine-mimicking 3D-featured hydrogels were modeled with Rhinoceros 5 software and 3D printed with a visible light DLP SLA printer (Titan 2 from Kudo3D, Taiwan) using a 45 s crosslinking time for every 100 μm layer. After 3D printing, non-crosslinked macromer and the dye was removed from the samples by immersing them in milli-Q water at RT with repeated water changes until no color was detected in the samples.

2.5 Physicochemical characterization of polymers and hydrogels

^{1}H NMR spectra of the digested dSIS and dSIS-MA polymers were recorded with a Bruker Avance III 700 MHz NMR spectrometer. Samples were dissolved in 0.01 N NaOD solution (7 mg/mL), and the spectrum was acquired in a 5 mm NMR tube at RT. The conversion of primary amine groups of lysine residues into methacrylamide groups was quantified with a colorimetric TNBS assay. Briefly, 0.6 mg of dSIS samples before and after methacryl-functionalization were added in 3 mL of 0.1 M sodium bicarbonate buffer (pH 8.5), which was then mixed with 1.5 mL of 0.01 % (w/v) TNBS in buffer. The solutions were incubated at 37 °C for 4 hours, after which 0.75 mL of 6 M HCl was added and the solutions were briefly incubated at 90°C to fully dissolve the samples. Blank samples were prepared similarly, except that the HCl was added before incubation with TNBS. The absorbance of the samples was measured at 300 - 600 nm using a UV-Vis spectrometer (Cary 8454, Agilent Technologies), after which the degree of functionalization (DOF) was calculated using Equation (1) with the absorbance values of dSIS ($A_{dSIS\text{-}MA}$) and dSIS-MA (A_{dSIS}) at 346 nm.[24]

$$DOF = (1 - A_{dSIS\text{-}MA} / A_{dSIS}) \times 100\% \qquad (1)$$

To study their secondary structure, the digested dSIS and dSIS-MA was first dissolved in a small amount of 0.01 N NaOH and then diluted in 7 mM phosphate buffer, after which the pH was adjusted with 0.01 N HCl to 7.4. The final polymer concentration was 0.1 mg/ml. 2 ml of the solution was added into a round cuvette with a 10 mm path length and scanned with a far-UV circular dichroism (CD) spectrometer (Olis™ DSM 20). The data was collected at 25 °C from 240 to 190 nm at 1 nm intervals with an averaging time of 0.5 s and number of increments of 100. For each sample, three measurements were averaged to obtain the final curve. The buffer background was subtracted from the spectra and the data was analyzed using the Olis Globalwork software. For calculating the mean residue ellipticity, the average molecular weight of 120 g/mol was used for the amino acids. Shear viscosity of the 3D printing

resins protected from light was analyzed using a rotational rheometer (Kinexus pro+, Malvern Panalytical) equipped with a 20 mm/1° cone plate geometry. Using a Peltier plate, temperature of the resin was increased from 20 °C to 40 °C with the heating rate of 0.5 °C/min, while the viscosity was measured at a constant shear rate of 1 Hz. A solvent trap was used for preventing water evaporation during the measurements. In addition, the stability of the resins at the printing temperature of 25°C was studied by measuring the viscosity at the shear rate of 1 Hz for 30 min. Furthermore, gelation kinetics of the resins under light exposure was measured with an Anton Paar modular compact rheometer (MCR 302) equipped with an 8 mm plate-to-plate geometry and a UV light curing system. The storage and loss moduli were determined at 20°C with an angular frequency of 1 rad/s, a shear strain of 1%, and a gap of 0.6 mm. The strain was determined from the linear viscoelastic regime (LVE-regime) in amplitude sweeps. The UV lamp having an intensity of 100 mW/cm^2 and equipped with a band-pass filter of 320-500 nm was turned on after 2 min of the measurement time. To measure a swelling ratio of the crosslinked materials, 3D printed disc samples were immersed in distilled water for 24 h to reach the swelling equilibrium, after which the samples were weighed, lyophilized, and weighed again. The swelling ratio was obtained by dividing the wet weight of a sample by its dry weight. The final mechanical properties of the 3D printed hydrogels after 24 h incubation at 37°C were studied with an oscillating rheometer (Kinexus pro+, Malvern Panalytical) using an 8 mm parallel plate geometry. First, the viscoelastic regime of wet samples (d = 8 mm, h = 2 mm) was determined with an amplitude sweep from a strain of 0.1% to 50% at 1 Hz, after which the storage modulus was measured with a frequency sweep from 0.1 Hz to 10 Hz at 37 °C using a 1% strain and a 0.1 N initial normal force.

Enzymatic biodegradation of the 3D printed, extracted hydrogels was evaluated by following the remaining mass of the samples immersed in collagenase II solution (1 U/mL in 50 mM $CaCl_2$, 5 mM MES buffer) at 37°C with an orbital shaking (30 rpm). The remaining mass percentage was calculated by dividing their wet weight at the predetermined time point by their initial wet weight after 24 h immersion in milli-Q water. The inside porosity of the hydrogels before degradation was visualized by cutting lyophilized samples in half and subsequently imaging the gold-coated samples with an SEM (Hitachi SU8030) at 15 kV. The local surface stiffness of the wet 3D printed hydrogels was mapped with NanoWizard4® atomic force microscopy (AFM, JPK Instruments, Berlin, Germany) at 37 °C. The device was mounted on an inverted optical microscope (LSM800, Zeiss, Oberkochen, Germany) with a temperature controller accessory. To measure the Young's modulus, samples with a diameter of 1 mm and a thickness of 0.5 mm were adhered on a petri dish in warm PBS. Triangular silicon nitride pyramidal tips attached to cantilevers with a nominal spring constant k = 0.35 N/m (SNL-10-A, Bruker, Mannheim, Germany) were calibrated by the thermal fluctuation method using the simple harmonic oscillator model on a bare petri dish and in PBS just prior to force spectroscopy experiments. A z-length of 2 µm, a rate of 2 µm/s, and a set point of 5 nN were used for the measurements. Controlled deformations were applied to the samples and the compressive feedback forces were measured through cantilever deflection. Force-displacement (F-Z) curves were produced by translating cantilever deflection (d) into force (F)

by means of F = kd, where k is the cantilever spring constant. The Young's modulus of the probed material was calculated by fitting the contact part of the measured approach force curves to a Hertz/Sneddon mechanics model for a triangular pyramidal indenter (tip) with a poisson's ratio of 0.5. The AFM was operated in a force spectroscopy contact mode, wherein an array 6 × 6 (32 points) of F–Z curves was collected over the entire scan area of 10 x 10 μm. For each sample, 250 to 400 sets of F–Z curves were collected for a better evaluation. Around 10% of curves were discarded for either loosing contact or with abnormal fluctuations in the baseline that cause a premature contact point identification. All data were processed using the AFM software package (JPK Instruments).

2.6 Culture and seeding of Caco-2 and HT29-mtx cells

Caco-2 and HT29-mtx cells were cultured in DMEM mixed with 20% or 10% FBS, respectively, and 1% non-essential amino acid solution and 1% penicillin/streptomycin antibiotic solution under standard conditions (5% CO_2, 37 °C, 95% humidity). The proliferation of Caco-2 cells on the crosslinked hydrogels was studied with PrestoBlue™ cell viability assay. Before cell seeding, 3D printed films (d = 5 mm, h = 0.4 mm) were treated with 70% ethanol for 1 h followed by immersion in PBS overnight with two changes of the PBS. Afterwards, the samples were placed in a 96-well plate and the cells (9.4 x 10^4 cells/cm^2) were seeded on top of the samples in 100 µL of media. At predetermined times, the metabolic activity of Caco-2 cells was measured by transferring the cell-covered samples to a new well plate and adding 100 µL of fresh medium with 10 µL of PrestoBlue™ solution into each well. After incubation for 2 h, the colored medium from each well was transferred to a new plate, and the absorbance was measured using a plate reader (Infinite® 200 PRO, Tecan) at 570 nm and at a 600 nm reference wavelength. Following the same cell seeding protocol as for the Caco-2 cells, HT29-mtx cells were seeded on the ethanol-treated hydrogel films with a seeding density of 1.56 x 10^5 cells/cm^2 and the co-culture of Caco-2/HT29-mtx cells were seeded on the 3D printed intestine-mimicking scaffolds with the ratio of 9:1 with a total seeding density of 9.4 x 10^4 cells/cm^2.

2.7 Generation of organoid-derived 2D monolayers on dSIS-MA hydrogels

Primary human epithelial cells were maintained *in vitro* as organoid cultures according to previously published protocols [25] as described in the supporting information. For organoid generation, the crypts were isolated from non-inflamed mucosa of the terminal ileum from resected Crohn's disease specimens, and the further human primary intestinal epithelial cells were derived from the organoid cultures of passage 5-10. Before cell seeding, the 3D printed dSIS-MA hydrogels (d = 5 mm, with or without 3D villi-mimics) were treated with 70% ethanol for 1 h followed by immersion in PBS (2 x 30 min), after which they were placed in 96-well plates and incubated overnight with advanced DMEM/F-12 medium supplemented with 20% fetal bovine serum, 2 mM L-glutamine, 50 units/ml penicillin, and 50 µg/ml streptomycin (base of organoid culture medium) at 4°C. The control substrates of Millicell™ inserts were placed in 12-well plates and coated at 4°C overnight with Matrigel™ diluted 1:10 in basal medium. Before seeding the cells, medium or coating solution was removed from the samples. Organoids grown for 5-7 days after passaging were collected by scraping off the

Matrigel™ domes with a pipette tip and transferring them into a 15-ml conical tube. Organoids were pelleted by centrifugation at 300 *g*, 4°C for 5 minutes and digested into single cells with TrypLE™ at 37°C. Every 5 minutes, the suspension was forced 10 times through a blunt 18G needle to aid digestion and monitored via light microscopy. After no more cell aggregates were visible (usually 15-25 minutes in TrypLE™), basal medium was added to stop the digestion process and the cells were centrifuged at 300 *g*, 4°C for 10 minutes. Subsequently, cells were washed once more with basal medium and resuspended in organoid culture medium supplemented with 10 µM Y-27632. The cell suspension was seeded on hydrogels or into inserts with 100 µl per well or 400 µl per insert corresponding to $3x10^5$ cells/cm^2. Culture medium was exchanged every 2 days and the monolayers were maintained in culture for 11 days before fixation and immunofluorescent analysis.

2.8 Immunofluorescence staining

The formation of tight junctions between the seeded Caco-2 or human primary cells were visualized by immunofluorescent (IF) staining of zonula occludens-1 (ZO-1) protein. The cell-covered samples were fixed with cold methanol for 5 min at 4 °C followed by two washes with PBS and then incubated in a blocking solution (5 wt-% of BSA in PBS/0.1% Tween buffer) for 1 h at RT. The cells were stained with ZO-1 primary antibody overnight at 4°C (1:250 in 1 wt-% BSA in PBS/0.1% Tween dilution buffer). After washing with PBS/0.1% Tween buffer (2 x 15 min), the samples were immersed in the secondary Alexa Fluor 647 antibody for 30 min at RT (1:400 in the dilution buffer), followed by Hoechst counterstaining for 5 min (1:2000 in PBS). Mucus production of HT29-mtx and human primary cells was detected by fixing the samples with 5% of formalin and staining the fixed cells with MUC5AC primary antibody (1: 200 in the dilution buffer) overnight at 4 °C and subsequently with secondary Alexa Fluor 488® antibody for 30 min at RT (1:400 in the dilution buffer). The nuclei and F-actin of the cells were counterstained with Hoechst (1:2000 in PBS) and Phalloidin-Atto 647® (1:100 in PBS), respectively, for 5 min at RT. The images were taken with a confocal microscope (LSM800, Carl Zeiss, Jena, Germany).

2.9 Statistical analysis

The statistical significance of the gathered data was determined using a Kruskal-Wallis test followed by Dunn's multiple comparisons test ($p < 0.05$), provided by Prism 9 software (GraphPad, USA).

3. Results

3.1 Solubilization and methacrylation of dSIS

To be able to use the dSIS in photocrosslinking-based SLA printing, we first solubilized and methacrylated the decellularized tissue. As shown in **Figure 1A**, the decellularization of SIS in subsequent SDS and Triton-X solutions resulted in fully colorless intestinal submucosa segments. The enzymatic digestion of the resulting dSIS with pepsin and the subsequent homogenization resulted in a transparent gel-like solution. The dsDNA content of the digested, lyophilized dSIS was 46 ± 1 ng/mg, locating below the generally accepted threshold

limit of 50 ng/mg.[26] The Quantibody® growth factor array showed the presence of various essential intestinal growth factors in the digested dSIS as listed in **Figure 1B** and **Table S1**, indicating preserved bioactivity of the material. The dry weight content of sGAG and hydroxyproline increased in the tissue after removal of the cells, while the enzymatic digestion decreased their content (**Figure 1B**). The further methacrylation of the digested dSIS did not significantly change the content of these biomolecules. During the functionalization of dSIS, the adjustment of the dSIS solution to pH 9 maintained the primary amines deprotonated and ready for reacting with the methacrylic anhydride and also decreased its viscosity, improving the stirring of the solution for homogenous functionalization. The functional group interconversion of the intrinsic, free lysine groups on dSIS into methacrylamides was evaluated with a colorimetric TNBS assay. Before the functionalization, the TNBS reagent reacted with free amino groups in the dSIS, forming a chromogenic derivative with an absorbance maximum at 346 nm (**Figure 1C**), while after it, drastically less chromogenic product was generated, revealing the DOF to be 88%. Furthermore, in the ^{1}H NMR spectra the peak *I* at 2.9 ppm assigned to the terminal methylene group in the lysine side chain in dSIS polymer disappeared and the peak *A* at 1.8 ppm and peaks *B* and *C* at 5.3 - 5.6 ppm assigned to the methacryloyl groups appeared (**Figure 1D**). Concluded both from the UV and NMR spectra, most of the amino end groups in the lysine side chains were converted to methacrylamides. The far-UV CD analysis of the secondary structure of dSIS and dSIS-MA in **Figure 1E** revealed the presence of triple helical structures both before and after methacrylation (the positive band around 220 nm), while the band indicating the random coil structure was less pronounced after the methacrylation (the negative band around 205 nm).

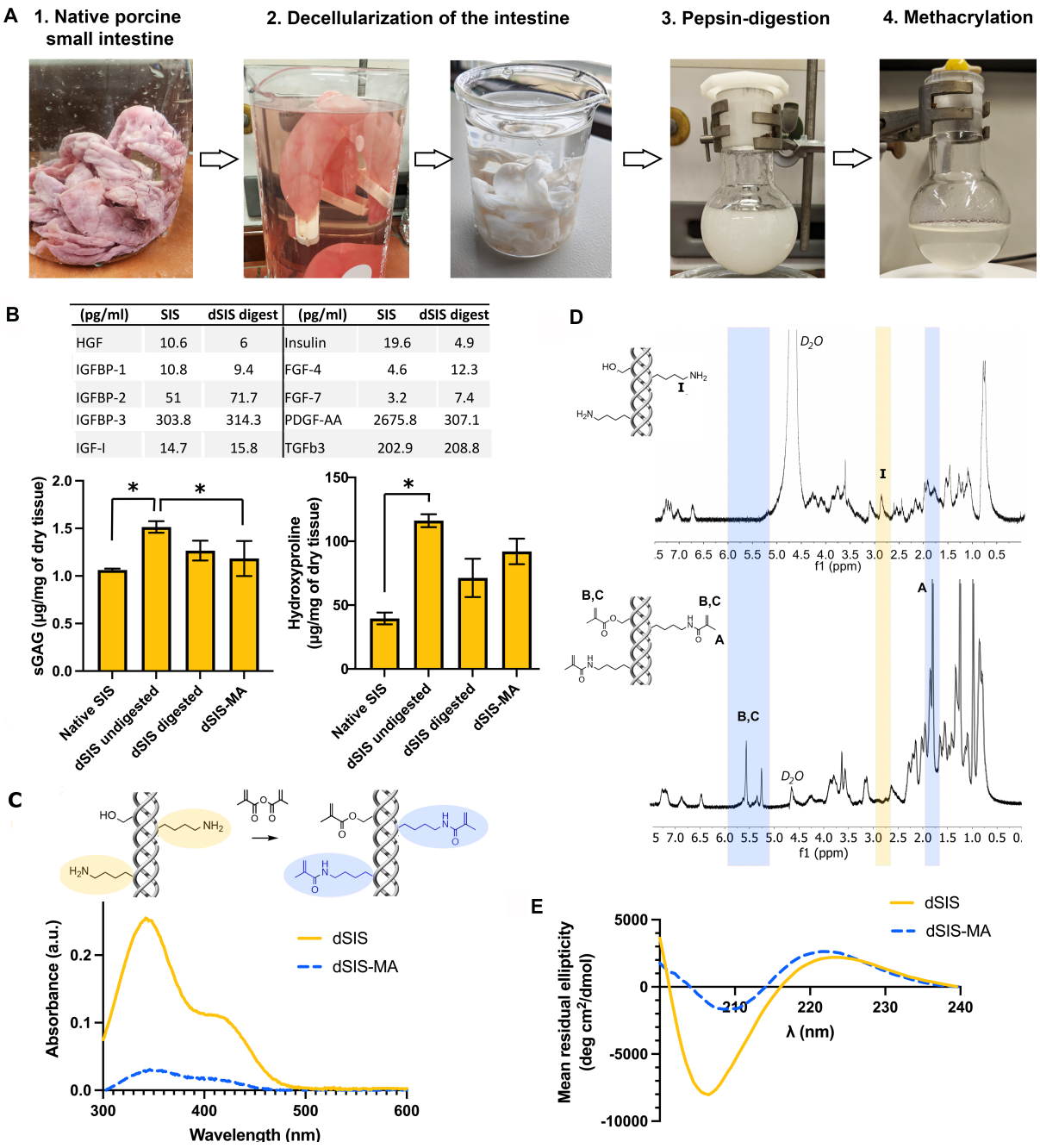

Figure 1. *Workflow of dSIS preparation and processing and its (bio)chemical characterization.* ***A****) Photographs of a small intestine-based material in the different phases of its processing into a photocrosslinkable polymer solution.* ***B****) Growth factor, sGAG, and hydroxyproline content of the native SIS and non-digested and digested dSIS (mean ± SD, n = 3, * indicates statistical significance (p < 0.05).* ***C****) A schematic presentation of the methacrylation of dSIS and representative UV-Vis spectra of the colorimetric TNBSA assay to derive the degree of functionalization and* ***D****) the representative ^{1}H NMR spectra of dSIS and dSIS-MA in 0.01N NaOD in D_2O (7 mg/mL).* ***E****) Representative far-UV CD spectra of the dSIS and dSIS-MA solutions (0.1 mg/mL in buffer at pH 7.4) to reveal the secondary structure of the polymers.*

3.2 Viscosity and crosslinking kinetics of the dSIS-MA resins and the swelling and mechanical properties of the photocrosslinked hydrogels

To enable the use of dSIS-MA in DLP SLA 3D printing, it was formulated into an aqueous photocrosslinkable resin in 0.01 N NaOH with various dSIS concentrations (1.5, 2, 2.5, and 3 wt-%). **Figure 2A** shows the change of the 1.5 wt-% resin from a viscous liquid to a transparent hydrogel when crosslinked with visible light in the SLA printer. As the free flow of the resin is a prerequisite in SLA printing, we studied its viscosity with a rotating rheometer using a temperature ramp from 20 °C to 40 °C (**Figure 2B**). For all the dSIS-MA concentrations, a similar viscosity pattern was detected: First, the viscosity slightly increased with temperature, until around 30°C it started dropping fast, particularly for the concentrations above 2 wt-%. The visual examination of the samples revealed the collapse of the resins at this point, resulting in the separation of the polymer from its aqueous medium. Therefore, the 3D printing temperature in SLA should remain below 30 °C to ensure the homogeneous composition of the resin during the printing process. To test the stability of the resins, their viscosity was measured for half an hour at 25 °C at the shear rate of 1 Hz (**Figure 2C**). Except for the highest concentration, the viscosity of the resins remained at a constant level, thus confirming their suitability for the SLA printing. The real-time measurement of the storage and loss modulus of the materials under UV light showed a steep increase in the storage modulus within the first minute, thereby revealing comparably fast reaction kinetics of the resins that is ideal for the SLA printing (**Figure 2D**). The lyophilized dSIS-MA hydrogels were highly porous (**Figure 2E**), and the pore size decreased in the µm-range with the increasing dSIS-MA concentration. The final elastic modulus of the hydrogels measured with an oscillating rheometer after a 24-hour immersion in PBS at 37 °C increased with the dSIS-MA concentration (**Figure 2F**) while the swelling ratio decreased (**Figure 2G**). The AFM analysis of the local stiffness on the wet hydrogel surfaces revealed also the Young's moduli to increase with the polymer concentration (**Figure 2H**). The dSIS-MA hydrogels constantly lost their mass in collagenase II solution at 37 °C, and the enzymatic degradation slowed down with the increasing dSIS-MA concentration (**Figure 2I**). However, the samples retained their shape until the last time point, after which the whole material dissolved into the solution and was no more weighable.

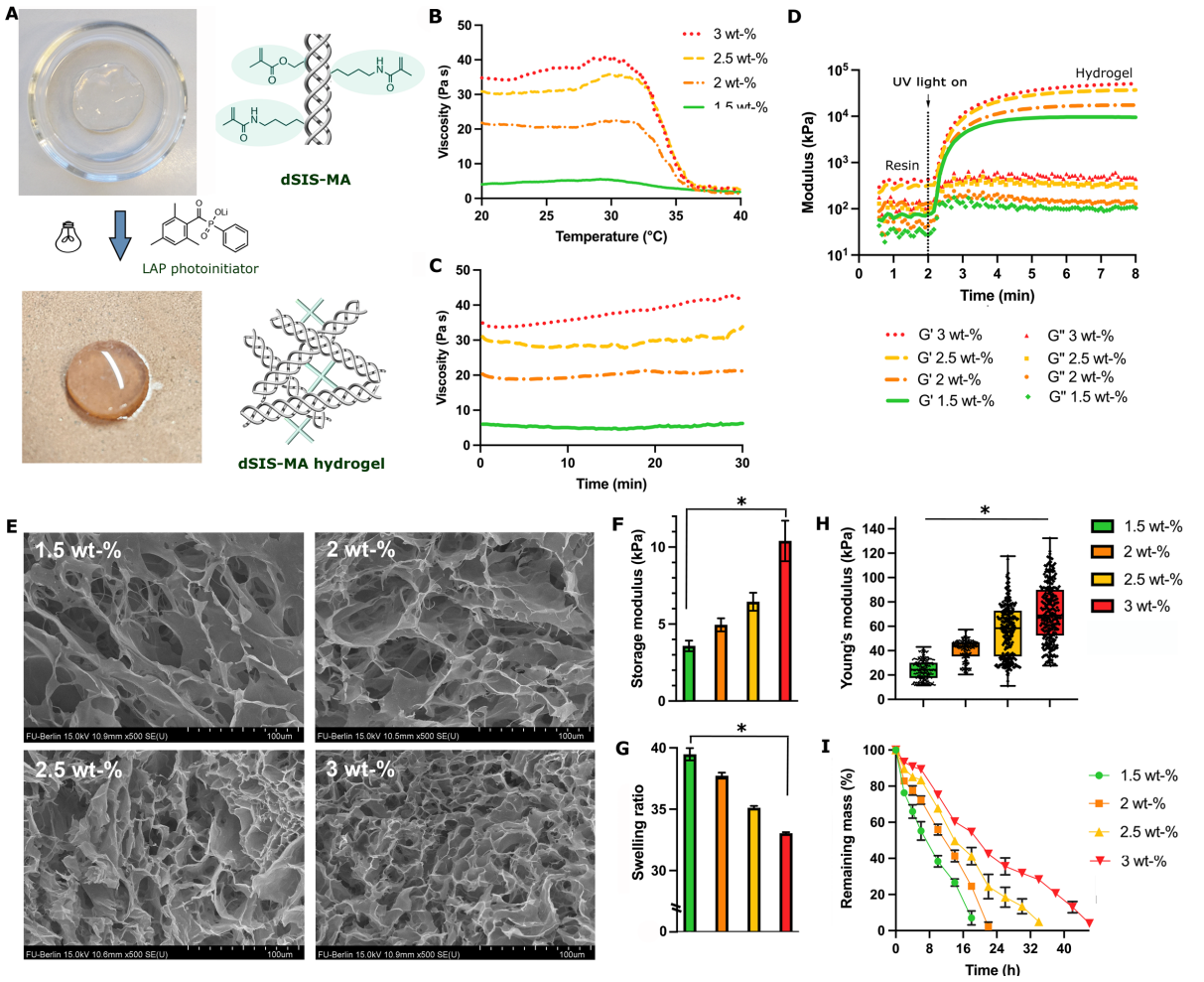

Figure 2. *Physicochemical characterization of the dSIS-MA resins and hydrogels.* ***A)*** *Photographs of dSIS-MA resin (1.5 wt-%) and the respective covalently crosslinked hydrogel.* ***B)*** *Temperature-dependent viscosity of the resins measured with a rotational rheometer at shear rate of 1 1/s and* ***C)*** *the stability of the viscosity at 25°C.* ***D)*** *Storage (G') and loss modulus (G'') of the resins and the resulting hydrogels before and after switching on the UV light.* ***E)*** *SEM images of the lyophilized hydrogels with various dSIS-MA concentrations showing the inner porosity of the samples.* ***F)*** *Final storage modulus measured with a plate rheometer and* ***G)*** *swelling ratio of the bulk wet hydrogels (mean ± SD, n = 3) as well as* ***H)*** *local Young's modulus of the wet hydrogel surfaces measured with AFM at 37°C.* ***I)*** *Enzymatic biodegradation of the wet hydrogels at 37 °C in collagenase II solution (1 U/mL) (mean ± SD, n = 3). * Indicates statistical significance (p < 0.05).*

3.3 Cytocompatibility of the photocrosslinked dSIS-MA hydrogels

As the new dSIS-based material was intended for 3D printing of intestinal tissue mimics, we studied its cell compatibility with intestinal epithelial cells. The proliferation of Caco-2 cells seeded on the flat hydrogels was followed with a colorimetric PrestoBlue™ metabolic activity assay (**Figure 3A**). For all the dSIS-MA concentrations, the cells covered the whole hydrogel surface regardless of its polymer concentration and no sign of toxicity of the materials in the form of reduced cell numbers or morphological changes was observed. Within the 7-day culture time, the metabolic activity of the cells increased on all the concentrations and was

higher on the hydrogels compared to the TCPS control. The IF staining of nuclei and tight junctional protein ZO-1 of the cells at day 7 showed the formation of a continuous tight junction barrier characteristic for epithelial cells (**Figure 3A** and **Figure S1**). As there was no significant difference in the metabolic activity and cell adhesion between the various dSIS-MA concentrations, the further cell culture studies were done with the softest hydrogels printed from the 1.5 wt-% dSIS-MA resin that most closely resembled the stiffness of human healthy intestinal tissue[27] and also had the most suitable viscosity for the SLA printing. Goblet-like HT29-mtx cells which are capable of mucin production – a critical attribute of advanced intestinal tissue models – were cultured on the 1.5 wt-% dSIS-MA hydrogels to study their functionality. Mucin 5AC secretion by HT29-mtx cells was confirmed after 11 days by IF staining (**Figure 3B** and **Figure S2**), revealing clear mucin production on the hydrogels similar to TCPS. Encouraged by the distinct adhesion and differentiation of the colon cancer-derived cell lines on the dSIS-MA hydrogels, we next seeded primary intestinal epithelial cells derived from human ileal organoids in their respective expansion medium. The IF staining of the nuclei and tight junctions of the primary cells at day 11 on the dSIS-MA hydrogels revealed full coverage of the samples by the proliferative cells as well as the formation of tight junctions and mucin 5AC in some of the cells (**Figure 3C**). The observed cell adhesion and functionality importantly indicated the suitability of our new material for biofabrication of primary cell-based small intestinal tissue mimics. As a comparison, the primary cells cultured on membrane inserts required a cell-adhesive precoating with Matrigel™ to form monolayers, and a more corrugated structure was observed on membranes with less mucin 5AC production compared to the monolayers on dSIS-MA hydrogels (**Figure 3D**).

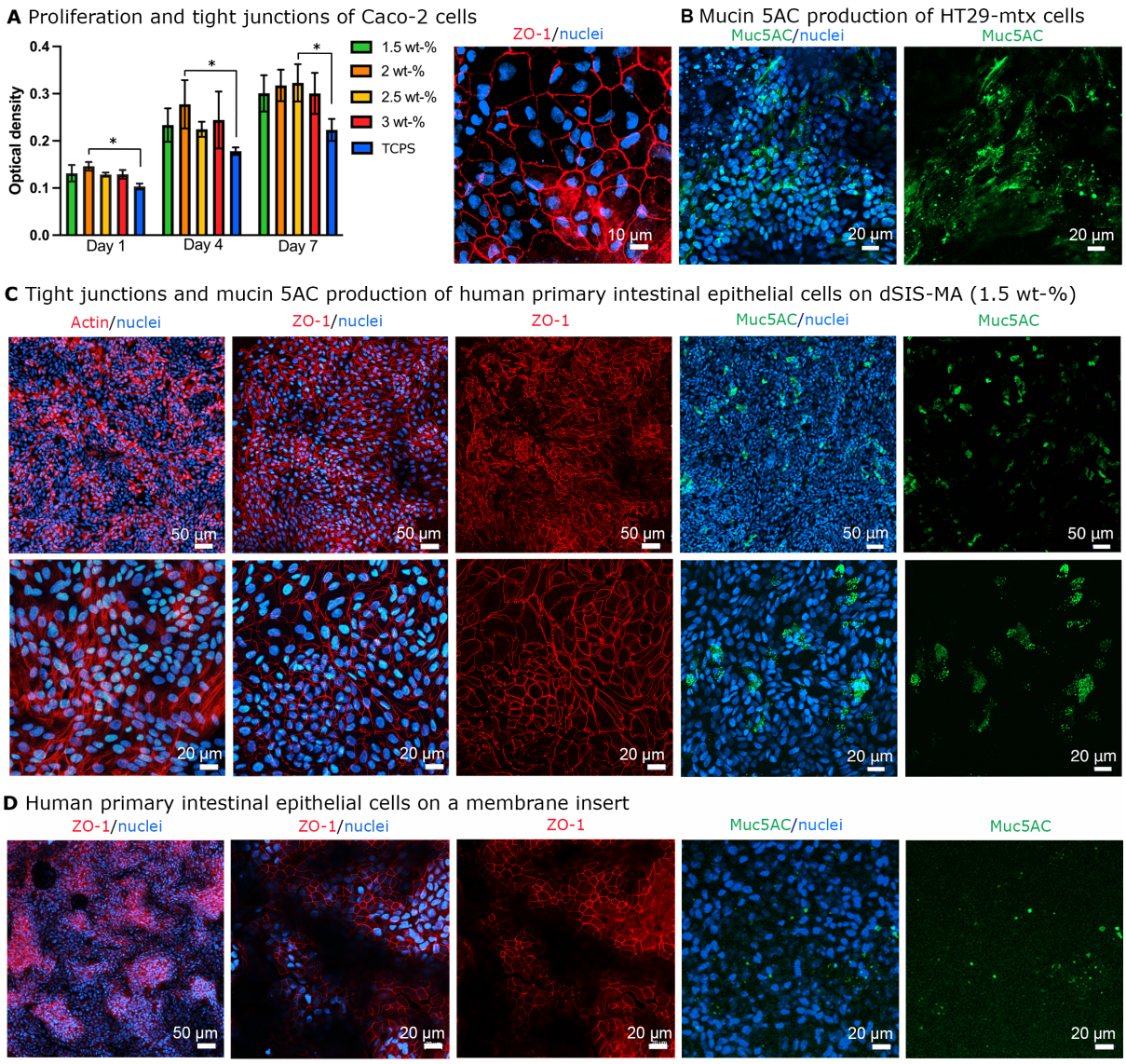

Figure 3. *Cell proliferation and mucin production on the dSIS-MA hydrogels.* ***A****) Time-dependent metabolic activity of Caco-2 cells seeded on a hydrogel surface of various dSIS concentrations and on a TCPS control (n = 4, errors indicate ± SD, * indicates significant difference (p < 0.05) and representative image of IF-stained nuclei and tight junctions of the cells on a 1.5 wt-% hydrogel at day 7. Further, representative images of* ***B****) HT29-mtx cells and* ***C****) human intestinal organoid-derived primary epithelial cells on 1.5 wt-% dSIS-MA hydrogels, and* ***D****) the primary cells seeded on Matrigel™-coated membrane inserts, all IF-stained for tight junctions and mucin 5AC after day 11 in culture.*

3.4 Biofabrication of the villi-mimicking hydrogel scaffolds

After confirming the desired cell attachment on the photocrosslinked dSIS-MA hydrogels, we used the resin consisting of 1.5 wt-% of dSIS-MA for 3D printing of CAD-modeled, intestine-mimicking scaffolds and seeded the undifferentiated human primary intestinal epithelial cells on these scaffolds as shown in **Figure 4A**. The array of villi-mimicking 3D structures was modelled on the intestinal scaffold (**Figure 4B**) to increase its surface area similar to the native intestinal epithelium, and the layer-by-layer 3D printing at RT resulted in hydrogels that closely replicated the modeled 3D scaffold (**Figure 4C**). The closer top view of the 3D printed

hydrogels photographed with a digital microscope camera (Conrad Components, Germany) showed the desired shape of the villi-mimicking structures (**Figure 4D**). To demonstrate the use of these scaffolds for growing epithelium-mimics, both a mixture of Caco-2/HT29-mtx cells (9:1) and organoid-derived human intestinal epithelial cells were seeded in their respective expansion medium on the hydrogel surface. The IF staining of the cell nuclei after 11 days of *in vitro* cell culture revealed both the cancer cell lines and the primary cells to cover the top surface of the villi-mimics. This was clearly seen in the z-stacks of confocal microscope images of the scaffolds (**Figures 4E** and **4F left**) and in the cross-sectional images of villi-structures (**Figures 4E** and **4F right**).

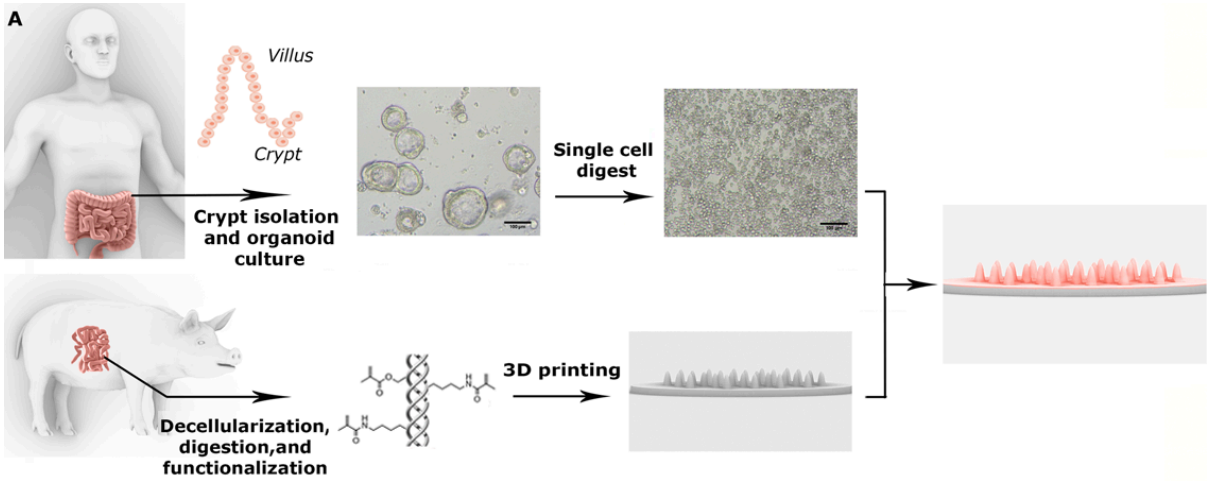

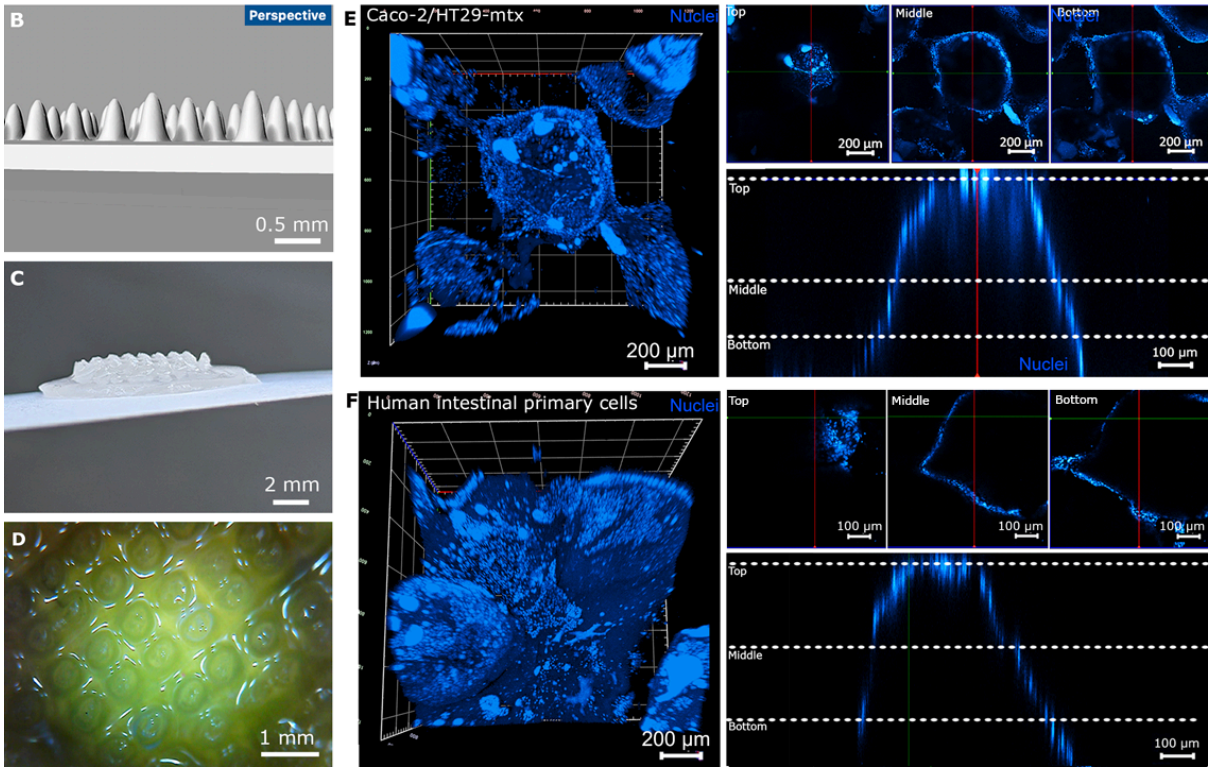

***Figure 4**. 3D printing of the intestinal scaffolds with villi-mimicking features and the subsequent cell seeding. **A**) A schematic presentation of the steps toward an intestinal tissue mimic, including the isolation of human primary intestinal epithelial cells and the formulation of dSIS-MA resin and its further 3D printing. **B**) A CAD model of a 3D scaffold mimicking villi structures on its luminal intestinal surface, **C**) a side view photograph and **D**) a top-view photograph of the 3D printed hydrogel after extraction in water. **E-F**) Representative confocal z-stack images of Hoechst-stained Caco-2/HT29-mtx cells (the bottom of the scaffold was excluded for better visualization of the villi mimics) and human intestinal epithelial cells seeded on top of the 3D printed scaffolds (images left) and the microscopy images of the cross-sections of cell-covered villi-mimics at different z-positions (Bottom, Middle, Top) and the respective orthogonal view where the dotted lines indicate the cutting planes (images right).*

4. Discussion

In our current work, we developed a new bioactive resin for 3D printing of physiology-mimicking tissue scaffolds that can be used especially for growing human intestinal tissue replicates. In a native small intestine, the epithelium is lined by polarized epithelial cells that form 3D structures called crypts and villi. The villi structures dramatically increases the area of the absorptive surface, while the crypts host the intestinal stem cells that constantly renew the epithelium.[29] Personalized *in vitro* replicates of this native intestinal epithelium hold potential for tissue replacement *in vivo* and are valuable *in vitro* platforms that allow uncomplicated studies of intestinal tissue development, homeostasis, and disease-related alterations. 3D printing is a great tool for building such *in vitro* tissue mimics as it allows straightforward, reproducible, and scalable fabrication of precisely designed complex 3D architectures. However, the successful 3D printing of tissue scaffolds requires an access to an ECM-mimicking 3D printing material that fulfills a unique set of certain biological, chemical, and physical properties. For this, we formulated a photocrosslinkable resin of the small intestine-derived dSIS-MA and demonstrated its potential by 3D printing of small intestine-mimicking scaffolds that we used for supporting growth of proliferative human primary intestinal epithelial cell.

Our new 3D printing resin was solely based on porcine dSIS tissue. The decellularization of SIS by successive treatment with anionic SDS and non-ionic Triton X-100 efficiently removed the porcine cells, making it nearly free from potentially immunogenic, xenogeneic DNA. We used pepsin-digestion to solubilize the dSIS as it cleaves the crosslink-containing terminal non-helical regions of collagen (*i.e.* telopeptides) and thereby makes the dSIS soluble without destroying its triple helix structure.[30] The pepsin-based digestion (1 mg pepsin/10 mg of dry dSIS, >2.5 kU/mg) resulted in homogeneous, fully solubilized dSIS after two days in acidic conditions at RT. Importantly, thorough grinding of the dSIS before the enzymatic digestion was essential as the presence of bigger parts tended to remarkably slow down the solubilization. Even though extending the digestion time of dSIS for longer than two days could have decreased the viscosity of the polymer resin especially in higher polymer concentrations, the prolonged digestion time has been seen to result in impaired cell compatibility of the final dECM hydrogels[31] and was therefore avoided. Interestingly, the

digested dSIS preserved its bioactivity in the form of sGAG molecules and various growth factors, such as FGF, HGF, IGF, PDGF, and TGF-ß, that are important for the regulation of intestinal cells and ECM.[32–35] The preserved growth factors have been previously reported also for liver dECM[36] and kidney dECM,[18] and for us it was a desired encouragement towards the further resin development as the presence of bioactive molecules differentiated our dSIS-MA from pure collagen.

The resin-based DLP SLA technique has typically a superior printing resolution compared to extrusion-based techniques as it is not limited by any extrusion head-related factors such as its speed, pressure, or size. Furthermore, the printing process is relatively fast and simple as there is no need for any multi-step mold preparations as required for example in micromolding biofabrication.[14] Provided that proper resins are available, even unsophisticated SLA printers like the one used in our current study can produce reasonable resolution for biofabrication and thus enables broad usage of the technique. The high degree of functionalization (88%) of the lysine end groups in dSIS during the methacrylation was desired as it enables fast and efficient photocrosslinking of the material in the SLA printing. The methacrylation decreased the water-solubility of the dSIS, which is why the resins were formulated in 0.01N NaOH solution to keep the collagen chains in dSIS apart from each other and the viscosity low enough for the SLA printing. We attributed the reduced water-solubility to the decreased number of positively charged amine groups in the dSIS-MA and to the intrinsic hydrophobicity of the formed methacrylamide groups. The suitable viscosity and photocrosslinking kinetics are among the most important characteristics of biomedical SLA resins besides their above-mentioned bioactivity. The concentration of 3 wt-% of dSIS-MA was the highest one to allow homogeneously mixed resins, while the concentration of 1.5 wt-% was the minimum to yield well-crosslinked hydrogels with an easy handling. Importantly, the viscosity of the resins of the lower concentrations remained stable for prolonged time at RT, which is critical in the SLA printing. The real-time rheological measurement of the resins under the UV light revealed their comparably fast crosslinking kinetics as the hydrogel samples in the rheometer were nearly fully crosslinked within the first minute. The hydrogels became softer after letting them saturate overnight in PBS at 37°C, and the final storage modulus of the water-equilibrated hydrogels ranged from 3.5 kPa to 10 kPa, the softest hydrogels almost resembling the stiffness of native human small intestine (2.9 kPa).[27] All the hydrogels regardless of their dSIS-MA concentration showed a high inner porosity, which in intestinal applications is important for the free nutrients flow and for establishing gradients of soluble biochemical factors through the material.[37] Interestingly, even though the photocrosslinked hydrogels constantly lost their mass and became softer in collagenase II solution, they did not lose their shape until they had fully biodegraded in the medium. This is important as it allows gradual reduction in the mechanical support to the maturing tissue while still maintaining the architectural features of the scaffold. The degradation rate was in good agreement with the one of photocrosslinked norbornene-functionalized collagen gels reported elsewhere,[38] and also confirmed that the covalent photocrosslinking via metacryl groups did not hinder the enzymatic degradation that is characteristic for the non-modified ECM materials.

Based on its low viscosity and the biomimicking stiffness of the resulting hydrogels, we 3D printed the CAD-modeled intestine-mimicking scaffolds using the 1.5 wt-% dSIS-MA resin. The full cell coverage and the lack of signs of toxicity indicated the cytocompatibility of the resulting 1.5 wt-% dSIS-MA hydrogels when tested both with cancer-derived intestinal cells and human intestinal organoid-derived cells. While all the cells formed a continuous tight junction barrier on the hydrogels, the HT29-mtx and primary cells additionally showed mucin 5AC production. This in good agreement with previous reports on HT29-mtx cells on porous filter membrane and glass or TCPS substrates.[39,40] The mucin 5AC produced by the HT29-mtx cells showed fibrous structure on the dSIS-MA hydrogels, whereas it appeared to be fully localized and stored in granules on TCPS, indicating some further bioactivity of the hydrogels. The organoid-derived undifferentiated primary cells were cultured on the 3D printed dSIS-MA scaffolds to demonstrate their *in vitro* epithelialization. Despite the existence of a myriad of human *in vitro* intestinal tissue models, the scarcity of models based on primary intestinal epithelial cells is due to their limited longevity and short life cycle.[41] For the prolonged culture of the primary intestinal cells, typical models are based on human or mice intestinal organoids generated from stem-cell containing small intestinal or colon crypts.[42–45] However, the closed organoids suffer from limited access of their epithelium, making the sampling and manipulation reliant on microinjections.[46,47] In our current work, we relied on techniques to generate confluent 2D monolayers from undifferentiated, proliferative organoid fragments with subsequent initiation of differentiation after reaching confluency.[48,49]. This concept has been previously applied on microfabricated collagen scaffolds to biofabricate human self-replicating colon and small intestinal jejunum models.[37,50] Our approach was to culture the primary, undifferentiated intestinal epithelial cells derived from human ileal organoids on the 3D printed dSIS-MA scaffolds mimicking the anatomical shape of the small intestinal epithelium. In our proof-of-concept studies, the cell growth until a confluency on the dSIS-MA hydrogels indicated the preserved proliferative capacity of these undifferentiated primary cells, thus featuring their stem cell character, which was supported by culturing them in L-WRN-conditioned expansion medium that provided the cells with the necessary growth factors.[22] Besides forming the tight junction barrier, a known feature of both undifferentiated and differentiated intestinal epithelial cells, some cells appeared to spontaneously differentiate into goblet-like cells without transfer to differentiation medium. Based on the mucin 5AC IF staining of the primary cells cultured on the dSIS-MA hydrogels and on the Matrigel®-coated filter membranes, a higher fractional number of cells seemed to differentiate spontaneously on the dSIS-MA samples, producing the mucin 5AC proteins. As mucin 5AC is typically predominantly expressed in the native stomach and to a lesser extent in the small intestine,[51] our future studies will focus on the cellular and mucin composition after transferring the tissue mimics into specific differentiation media and under the dynamic medium flow. Even though the indefinitely growing cancer cell lines, Caco-2 and HT29-mtx cells, are a great help in developing simple intestinal tissue models, their various non-physiological characteristics reduce their biological relevancy.[52] Therefore, the demonstrated capacity to grow primary intestinal cells on the dSIS-MA scaffolds significantly improves the physiological relevancy of

the resulting tissue mimics. Furthermore, the opportunity of using human tissue biopsies and biobanks as a cell source instead of tumor cell lines enables the development of personalized human disease models for the improved understanding of patient-specific pathophysiology and drug testing.

5. Conclusions

We formulated a new bioactive, photocrosslinkable 3D printing resin based on dSIS methacrylamide and used it for 3D printing of small intestine-mimicking tissue scaffolds. When diluted to a low concentration (1.5 wt-%), the aqueous resin exhibited both the viscosity and the photocrosslinking kinetics suitable for the comparably simple and low-cost DLP SLA printing. The highly swelling but also durable dSIS-MA hydrogels supported the adhesion and proliferation of seeded human primary intestinal epithelial cells without requirement for additional pre-coatings. The 3D printed intestinal tissue scaffolds exhibited a biomimicking elasticity and intrinsic bioactivity that was highlighted by the spontaneous differentiation of the intestinal organoid-derived stem cells into mucus producing goblet cells without exposure to typical differentiation media. Based on its excellent 3D printing properties and supportive nature in the culture of intestinal epithelial cells, we envision the new dSIS-MA resin to greatly help with engineering more advanced *in vitro* tissue mimics of an enhanced biomimicry and physiological relevancy. The physiologically shaped intestinal tissue mimics with a free access to their epithelium would benefit the wide spectrum of biomedical, pharmaceutical, and tissue engineering research after spatially controlled differentiation of the confluent epithelial cell layer.

Acknowledgement

The authors warmly thank Dahlem Research School and the Focus Area Nanoscale at Freie Universität Berlin (LE), the Federal Ministry of Education and Research (FKZ: 13N13523) (MW), the German Research Foundation (DFG; SFB1449-B04/Z02) (MW, LH, AA, BS) for the financial support of the current work and M.Sc. Peng Tang for taking the SEM images at the Core Facility of BioSupraMol supported by the German Research Foundation (DFG). Dr. Karl Hillebrandt is participant in the BIH Charité Clinician Scientist Program funded by the Charité – Universitätsmedizin Berlin, and the Berlin Institute of Health at Charité (BIH). The authors further acknowledge the support of the Cluster of Excellence »Matters of Activity. Image Space Material« funded by the Deutsche Forschungsgemeinschaft (DFG, German Research Foundation) under Germany's Excellence Strategy (EXC 2025).

References

[1] Z. Wang, R. Abdulla, B. Parker, R. Samanipour, S. Ghosh, K. Kim, A simple and high-resolution stereolithography-based 3D bioprinting system using visible light crosslinkable bioinks, Biofabrication. 7 (2015) 45009. https://doi.org/10.1088/1758-5090/7/4/045009.

[2] B. Yue, Biology of the Extracellular Matrix: An Overview, J. Glaucoma. 23 (2014) S20. https://doi.org/10.1097/IJG.0000000000000108.

[3] S.H. Kim, J. Turnbull, S. Guimond, Extracellular matrix and cell signalling: The dynamic

cooperation of integrin, proteoglycan and growth factor receptor, J. Endocrinol. 209 (2011) 139–151. https://doi.org/10.1530/JOE-10-0377.

[4] B. Struecker, A. Butter, K. Hillebrandt, D. Polenz, A. Reutzel-Selke, P. Tang, S. Lippert, A. Leder, S. Rohn, D. Geisel, T. Denecke, K. Aliyev, K. Jöhrens, N. Raschzok, P. Neuhaus, J. Pratschke, I.M. Sauer, Improved Rat Liver Decellularization by Arterial Perfusion Under Oscillating Pressure Conditions, J. Tissue Eng. Regen. Med. 11 (2017) 531–541. https://doi.org/10.1002/term.1948.

[5] G. Cao, Y. Huang, K. Li, Y. Fan, H. Xie, X. Li, Small intestinal submucosa: Superiority, limitations and solutions, and its potential to address bottlenecks in tissue repair, J. Mater. Chem. B. 7 (2019) 5038–5055. https://doi.org/10.1039/c9tb00530g.

[6] X. Zhang, Z. Fang, E. Cho, K. Huang, J. Zhao, J. Jiang, X. Huangfu, Use of a novel, reinforced, low immunogenic, porcine small intestine submucosa patch to repair a supraspinatus tendon defect in a rabbit model, Biomed Res. Int. 2019 (2019). https://doi.org/10.1155/2019/9346567.

[7] F. Wang, Q. Song, L. Du, X. Wu, Development and Characterization of an Acellular Porcine Small Intestine Submucosa Scaffold for Use in Corneal Epithelium Tissue Engineering, Curr. Eye Res. 45 (2020) 134–143. https://doi.org/10.1080/02713683.2019.1663386.

[8] M. Schweinlin, S. Wilhelm, I. Schwedhelm, J. Hansmann, R. Rietscher, C. Jurowich, H. Walles, M. Metzger, Development of an advanced primary human in vitro model of the small intestine, Tissue Eng. - Part C Methods. 22 (2016) 873–883. https://doi.org/10.1089/ten.tec.2016.0101.

[9] M. Schweinlin, A. Rossi, N. Lodes, C. Lotz, S. Hackenberg, M. Steinke, H. Walles, F. Groeber, Human barrier models for the in vitro assessment of drug delivery, Drug Deliv. Transl. Res. 7 (2017) 217–227. https://doi.org/10.1007/s13346-016-0316-9.

[10] M. Alzheimer, S.L. Svensson, F. König, M. Schweinlin, M. Metzger, H. Walles, C.M. Sharma, A three-dimensional intestinal tissue model reveals factors and small regulatory RNAs important for colonization with Campylobacter jejuni, 2020. https://doi.org/10.1371/journal.ppat.1008304.

[11] W.J. Kim, G.H. Kim, An intestinal model with a finger-like villus structure fabricated using a bioprinting process and collagen/SIS-based cell-laden bioink, Theranostics. 10 (2020) 2495–2508. https://doi.org/10.7150/thno.41225.

[12] L. Shi, Y. Hu, M.W. Ullah, I. Ullah, H. Ou, W. Zhang, L. Xiong, X. Zhang, Cryogenic free-form extrusion bioprinting of decellularized small intestinal submucosa for potential applications in skin tissue engineering, Biofabrication. 11 (2019). https://doi.org/10.1088/1758-5090/ab15a9.

[13] T. Hiller, J. Berg, L. Elomaa, V. Röhrs, I. Ullah, K. Schaar, A.-C. Dietrich, M. Al-Zeer, A. Kurtz, A. Hocke, S. Hippenstiel, H. Fechner, M. Weinhart, J. Kurreck, Generation of a 3D Liver Model Comprising Human Extracellular Matrix in an Alginate/Gelatin-Based Bioink by Extrusion Bioprinting for Infection and Transduction Studies, Int. J. Mol. Sci. 19 (2018) 3129. https://doi.org/10.3390/ijms19103129.

[14] Y. Wang, D.B. Gunasekara, M.I. Reed, M. Disalvo, S.J. Bultman, C.E. Sims, S.T. Magness, N.L. Allbritton, A microengineered collagen scaffold for generating a polarized crypt- villus architecture of human small intestinal epithelium, Biomaterials.

128 (2017) 44–55. https://doi.org/10.1016/j.biomaterials.2017.03.005.

[15] J.A. Serna, S.L. Florez, V.A. Talero, J.C. Briceño, C. Muñoz-Camargo, J.C. Cruz, Formulation and characterization of a SIS-Based photocrosslinkable bioink, Polymers (Basel). 11 (2019) 1–10. https://doi.org/10.3390/polym11030569.

[16] J. Visser, P.A. Levett, N.C.R. te Moller, J. Besems, K. Boere, M.H.P. van Rijen, J.C. de Grauw, W.J.. Dhert, P.R. van Weeren, J. Malda, Crosslinkable Hydrogels Derived from Cartilage, Meniscus, and Tendon Tissue, Tissue Eng. Part A. 21 (2015) 1195–206. https://doi.org/10.1089/TEN.TEA.2014.0362.

[17] B.B. Rothrauff, L. Coluccino, R. Gottardi, L. Ceseracciu, S. Scaglione, L. Goldoni, R.S. Tuan, Efficacy of Thermoresponsive, Photocrosslinkable Hydrogels Derived from Decellularized Tendon and Cartilage Extracellular Matrix for Cartilage Tissue Engineering, J. Tissue Eng. Regen. Med. 12 (2018) e159–e170. https://doi.org/10.1002/term.2465.

[18] M. Ali, A.K. PR, J.J. Yoo, F. Zahran, A. Atala, S.J. Lee, A Photo-Crosslinkable Kidney ECM-Derived Bioink Accelerates Renal Tissue Formation, Adv. Healthc. Mater. 8 (2019) 1800992. https://doi.org/10.1002/adhm.201800992.

[19] W. Kim, H. Lee, J. Lee, A. Atala, J.J. Yoo, S. Jin, G.H. Kim, Efficient myotube formation in 3D bioprinted tissue construct by biochemical and topographical cues, Biomaterials. 230 (2020) 119632. https://doi.org/10.1016/j.biomaterials.2019.119632.Efficient.

[20] X. Ma, C. Yu, P. Wang, W. Xu, X. Wan, C.S.E. Lai, J. Liu, A. Koroleva-Maharajh, S. Chen, Rapid 3D bioprinting of decellularized extracellular matrix with regionally varied mechanical properties and biomimetic microarchitecture, Biomaterials. 185 (2018) 310–321. https://doi.org/10.1016/j.biomaterials.2018.09.026.

[21] L. Elomaa, E. Keshi, I.M. Sauer, M. Weinhart, Development of GelMA/PCL and dECM/PCL resins for 3D printing of acellular in vitro tissue scaffolds by stereolithography, Mater. Sci. Eng. C. 112 (2020) 110958. https://doi.org/10.1016/J.MSEC.2020.110958.

[22] H. Miyoshi, T.S. Stappenbeck, In vitro expansion and genetic modification of gastrointestinal stem cells as organoids, Nat. Protoc. 8 (2013) 1–24. https://doi.org/10.1038/nprot.2013.153.In.

[23] V. Coulson-Thomas, T. Gesteira, Dimethylmethylene Blue Assay (DMMB), Bio-Protocol. 4 (2014) 1–5. https://doi.org/10.21769/bioprotoc.1236.

[24] R. Ravichandran, M.M. Islam, E.I. Alarcon, A. Samanta, S. Wang, P. Lundström, J. Hilborn, M. Griffith, J. Phopase, Functionalised type-I collagen as a hydrogel building block for bio-orthogonal tissue engineering applications, J. Mater. Chem. B. 4 (2015) 318–326. https://doi.org/10.1039/c5tb02035b.

[25] C. Pleguezuelos-Manzano, J. Puschhof, S. van den Brink, V. Geurts, J. Beumer, H. Clevers, Establishment and Culture of Human Intestinal Organoids Derived from Adult Stem Cells, Curr. Protoc. Immunol. 130 (2020). https://doi.org/10.1002/cpim.106.

[26] P.M. Crapo, T.W. Gilbert, S.F. Badylak, An overview of tissue and whole organ decellularization processes, Biomaterials. 32 (2012) 3233–3243. https://doi.org/10.1016/j.biomaterials.2011.01.057.An.

[27] L.A. Johnson, E.S. Rodansky, K.L. Sauder, J.C. Horowitz, J.D. Mih, D.J. Tschumperlin, P.D. Higgins, Matrix stiffness corresponding to strictured bowel induces a fibrogenic response in human colonic fibroblasts, Inflamm. Bowel Dis. 19 (2013) 891–903. https://doi.org/10.1097/MIB.0b013e3182813297.

[28] G. Linz, S. Djeljadini, L. Steinbeck, G. Köse, F. Kiessling, M. Wessling, Cell barrier characterization in transwell inserts by electrical impedance spectroscopy, Biosens. Bioelectron. 165 (2020) 112345. https://doi.org/10.1016/j.bios.2020.112345.

[29] N. Barker, J.H. Van Es, J. Kuipers, P. Kujala, M. Van Den Born, M. Cozijnsen, A. Haegebarth, J. Korving, H. Begthel, P.J. Peters, H. Clevers, Identification of stem cells in small intestine and colon by marker gene Lgr5, Nature. 449 (2007) 1003–1007. https://doi.org/10.1038/nature06196.

[30] J. Qian, Y. Okada, T. Ogura, K. Tanaka, S. Hattori, S. Ito, J. Satoh, T. Takita, K. Yasukawa, Kinetic Analysis of the Digestion of Bovine Type I Collagen Telopeptides with Porcine Pepsin, J. Food Sci. 81 (2016) C27–C34. https://doi.org/10.1111/1750-3841.13179.

[31] R.A. Pouliot, B.M. Young, P.A. Link, H.E. Park, A.R. Kahn, K. Shankar, M.B. Schneck, D.J. Weiss, R.L. Heise, Porcine Lung-Derived Extracellular Matrix Hydrogel Properties Are Dependent on Pepsin Digestion Time, Tissue Eng Part C Methods. 26 (2020) 332–346. https://doi.org/10.1089/ten.TEC.2020.0042.

[32] A.U. Dignass, A. Sturm, Peptide growth factors in the intestine, Eur. J. Gastroenterol. Hepatol. 13 (2001) 763–770. https://doi.org/10.1097/00042737-200107000-00002.

[33] S.Y. Koyama, D.K. Podolsky, beta in rat intestinal epithelial cells ., 83 (1989) 1768–1773.

[34] M. Kurokowa, K. Lynch, D.K. Podolsky, Effects of growth factors on an intestinal epithelial cell line: Transforming growth factor β inhibits proliferation and stimulates differentiation, Biochem. Biophys. Res. Commun. 142 (1987) 775–782. https://doi.org/10.1016/0006-291X(87)91481-1.

[35] M. Laburthe, C. Rouyer-Fessard, S. Gammeltoft, Receptors for insulin-like growth factors I and II in rat gastrointestinal epithelium, Am. J. Physiol. - Endocrinol. Metab. 254 (1988). https://doi.org/10.1152/ajpgi.1988.254.3.g457.

[36] A. Skardal, L. Smith, S. Bharadwaj, A. Atala, S. Soker, Y. Zhang, Tissue specific synthetic ECM hydrogels for 3-D in vitro maintenance of hepatocyte function, Biomaterials. 33 (2012) 4565–4575. https://doi.org/10.1016/j.biomaterials.2012.03.034.

[37] Y. Wang, D.B. Gunasekara, M.I. Reed, M. DiSalvo, S.J. Bultman, C.E. Sims, S.T. Magness, N.L. Allbritton, A microengineered collagen scaffold for generating a polarized crypt-villus architecture of human small intestinal epithelium, Biomaterials. 128 (2017) 44–55. https://doi.org/10.1016/j.biomaterials.2017.03.005.

[38] K. Guo, H. Wang, S. Li, H. Zhang, S. Li, H. Zhu, Z. Yang, L. Zhang, P. Chang, X. Zheng, Collagen-Based Thiol-Norbornene Photoclick Bio-Ink with Excellent Bioactivity and Printability, ACS Appl. Mater. Interfaces. 13 (2021) 7037–7050. https://doi.org/10.1021/acsami.0c16714.

[39] N. Navabi, M.A. McGuckin, S.K. Lindén, Gastrointestinal Cell Lines Form Polarized Epithelia with an Adherent Mucus Layer when Cultured in Semi-Wet Interfaces with

Mechanical Stimulation, PLoS One. 8 (2013). https://doi.org/10.1371/journal.pone.0068761.

[40] M. Lindner, A. Laporte, S. Block, L. Elomaa, M. Weinhart, Physiological shear stress enhances differentiation, mucus-formation and structural 3d organization of intestinal epithelial cells in vitro, Cells. 10 (2021). https://doi.org/10.3390/cells10082062.

[41] J. Grossmann, K. Walther, M. Artinger, S. Kiessling, M. Steinkamp, W.K. Schmautz, F. Stadler, F. Bataille, M. Schultz, J. Schsolmerich, G. Rogler, Progress on isolation and short-term ex-vivo culture of highly purified non-apoptotic human intestinal epithelial cells (IEC), Eur. J. Cell Biol. 82 (2003) 262–270. https://doi.org/10.1078/0171-9335-00312.

[42] T. Sato, D.E. Stange, M. Ferrante, R.G.J. Vries, J.H. Van Es, S. Van Den Brink, W.J. Van Houdt, A. Pronk, J. Van Gorp, P.D. Siersema, H. Clevers, Long-term expansion of epithelial organoids from human colon, adenoma, adenocarcinoma, and Barrett's epithelium, Gastroenterology. 141 (2011) 1762–1772. https://doi.org/10.1053/j.gastro.2011.07.050.

[43] M. Almeqdadi, M.D. Mana, J. Roper, Ö.H. Yilmaz, Gut organoids: Mini-tissues in culture to study intestinal physiology and disease, Am. J. Physiol. - Cell Physiol. 317 (2019) C405–C419. https://doi.org/10.1152/ajpcell.00300.2017.

[44] J. Sprangers, I.C. Zaalberg, M.M. Maurice, Organoid-based modeling of intestinal development, regeneration, and repair, Cell Death Differ. 28 (2021) 95–107. https://doi.org/10.1038/s41418-020-00665-z.

[45] G. Altay, E. Larrañaga, S. Tosi, F.M. Barriga, E. Batlle, V. Fernández-Majada, E. Martínez, Self-organized intestinal epithelial monolayers in crypt and villus-like domains show effective barrier function., Sci. Rep. 9 (2019) 10140. https://doi.org/10.1038/s41598-019-46497-x.

[46] J. Puschhof, C. Pleguezuelos-Manzano, A. Martinez-Silgado, N. Akkerman, A. Saftien, C. Boot, A. de Waal, J. Beumer, D. Dutta, I. Heo, H. Clevers, Intestinal organoid cocultures with microbes, Nat. Protoc. 16 (2021) 4633–4649. https://doi.org/10.1038/s41596-021-00589-z.

[47] Q. He, J. Johnston, J. Zeitlinger, K. City, K. City, A Small Intestinal Organoid Model of Non-invasive Enteric Pathogen-Epithelial Cell Interactions, Mucosal Immunol. 33 (2015) 395–401. https://doi.org/10.1038/mi.2014.72.A.

[48] P. Hoffmann, N. Schnepel, M. Langeheine, K. Kunnemann, G.A. Grassl, R. Brehm, B. Seeger, G. Mazzuoli-Weber, G. Breves, Intestinal organoid-based 2D monolayers mimic physiological and pathophysiological properties of the pig intestine, PLoS One. 16 (2021) 1–15. https://doi.org/10.1371/journal.pone.0256143.

[49] Y. Wang, M. DiSalvo, D.B. Gunasekara, J. Dutton, A. Proctor, M.S. Lebhar, I.A. Williamson, J. Speer, R.L. Howard, N.M. Smiddy, S.J. Bultman, C.E. Sims, S.T. Magness, N.L. Allbritton, Self-renewing Monolayer of Primary Colonic or Rectal Epithelial Cells, Cell. Mol. Gastroenterol. Hepatol. 4 (2017) 165-182.e7. https://doi.org/10.1016/J.JCMGH.2017.02.011.

[50] S.S. Hinman, Y. Wang, R. Kim, N.L. Allbritton, In vitro generation of self-renewing human intestinal epithelia over planar and shaped collagen hydrogels, Nat. Protoc. 16

(2021) 352–382. https://doi.org/10.1038/s41596-020-00419-8.

[51] A.M. Rodríguez-Piñeiro, J.H. Bergström, A. Ermund, J.K. Gustafsson, A. Schütte, M.E.V. Johansson, G.C. Hansson, Studies of mucus in mouse stomach, small intestine, and colon. II. Gastrointestinal mucus proteome reveals Muc2 and Muc5ac accompanied by a set of core proteins, Am. J. Physiol. - Gastrointest. Liver Physiol. 305 (2013) 348–356. https://doi.org/10.1152/ajpgi.00047.2013.

[52] H. Sun, E.C.Y. Chow, S. Liu, Y. Du, K.S. Pang, The Caco-2 cell monolayer: Usefulness and limitations, Expert Opin. Drug Metab. Toxicol. 4 (2008) 395–411. https://doi.org/10.1517/17425255.4.4.395.